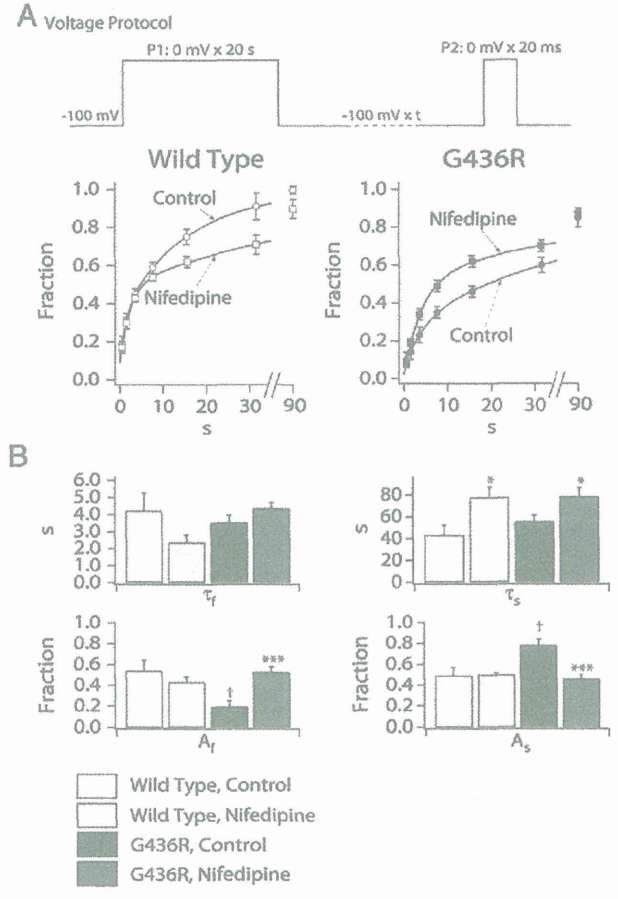

Fig. 5. Effect of nifedipine on recovery of LTCC (WT) and LTCC (G436R) channels at −100 mV. (A) Top panel: voltage protocol. Bottom panels: the recovery from inactivation of LTCC (WT) and LTCC (G436R) channels at −100 mV in the absence and presence of 3 nmol/L nifedipine. Peak amplitude of LTCC currents in P2 was normalized to that in P1, and plotted against the duration between P1 and P2. Symbols and bars indicate the mean ± S.E.M. Lines are the fit of the data with Eq. (4). (B) Parameters used to fit Eq. (4) to the time course of the recovery from inactivation of LTCC (WT) and LTCC (G436R) channels in the presence and absence of nifedipine (Table 1). Data are shown as the means ± S.E.M. *: P<0.05 vs. CONT; ***: P<0.001 vs. CONT; †: P<0.05 vs. WT.

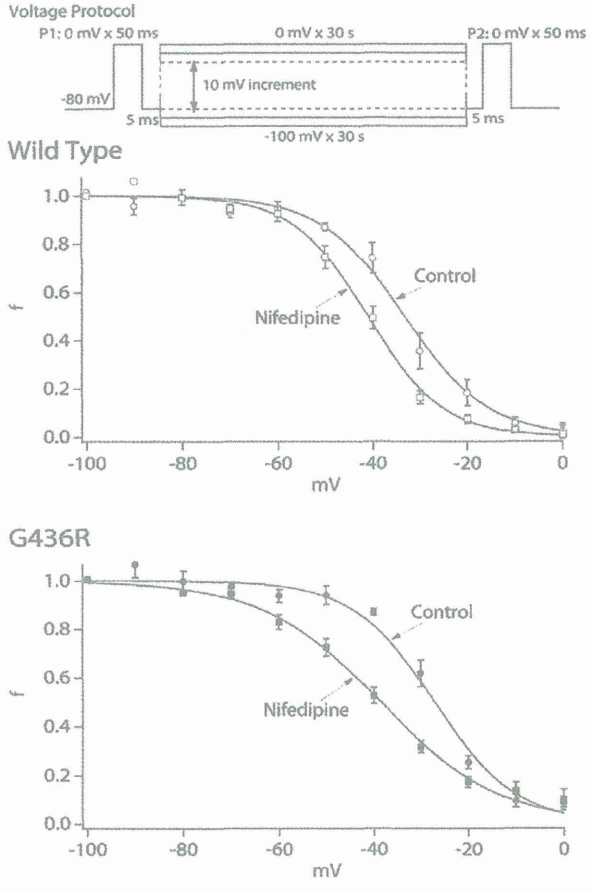

Fig. 6. Effect of nifedipine on isochronal inactivation of LTCC (WT) and LTCC (G436R) channels. Top panel: voltage protocol. Middle and bottom panels: isochronal inactivation of LTCC (WT) and LTCC (G436R) in the absence and presence of 3 nmol/L nifedipine. Peak LTCC current amplitude in P2 was normalized to that in P1 (f) and plotted against membrane potentials. Symbols and bars indicate the mean ± S.E.M. Lines are the fit of the data with Eq. (5) with parameters summarized in Table 1.

pulses to different membrane potentials (Fig. 6). Lines are the fit of the averaged data with a Boltzmann function (Eq. (5)). Neither the half-maximum inactivation potential nor a slope factor was significantly different between LTCC (WT) and LTCC (G436R) channels in the absence of nifedipine (Table 1). Nifedipine significantly caused a leftward shift of the inactivation curve by ~7 mV in the LTCC (WT) channels and by ~11 mV in the LTCC (G436R) channels.

4. Discussion

4.1. Model of $Ca_V1.2$ L-type Ca^{2+} channels

Both LTCC (WT) and LTCC (G436R) exhibited biexponential CSI (Fig. 3), OSI (Fig. 4) and recovery from OSI (Fig. 5), indicating that they may have fast and slow VDI sates. Fig. 7A illustrates the minimum state diagram of LTCCs. C_0 is a closed state occurring at deeply hyperpolarized potentials whereas C_4 is a pre-open closed state prevailing at the sub-threshold potential (Yarotskyy et al., 2009). Upon depolarization from hyperpolarized potentials to supra-threshold potentials, LTCCs transit from C_0 to C_4 and then to an open state (O). Each closed and open state is connected with fast inactivated states (I_{cf0}–I_{cf4}, I_{of}) and slow inactivated states (I_{cs0}–I_{cs4}, I_{os}). Nifedipine independently binds to each state (asterisks).

4.2. Comparison of LTCC (WT) and LTCC (G436R) channels in the absence of nifedipine

LTCC (WT) and LTCC (G436R) were activated at potentials positive to −30 mV and exhibited an almost identical current–voltage-relationship (Fig. 1), indicating that activation (C_0–O) is similar in these channels. It was reported that LTCC (G436R) channels exhibited slower activation and deactivation than LTCC (WT) channels (Yarotskyy et al., 2009); however, the steady-state activation does not seem to be significantly different between these channels.

At −40 mV, most LTCCs may transit from C_4 to I_{cf4} and I_{cs4} (Fig. 7A). LTCC (G436R) exhibited smaller A_f than LTCC (WT) (Fig. 3), indicating that the mutation selectively impairs I_{cf4} and thus, that L_{I-II} supports I_{cf4}. Yarotskyy et al. (2009) reported that the G436R mutation did not affect CSI at −60 mV. Thus, L_{I-II} seems to support fast CSI at potentials positive to the sub-threshold potential. At 0 mV, LTCCs exhibited OSI (O–I_{of}, O–I_{os}) (Fig. 7A). We found stronger OSI of LTCC (G436R) than previously reported (Fig. 4) (Barrett and Tsien, 2008; Raybaud et al., 2006; Splawski et al., 2004; Yarotskyy et al., 2009), probably due to the higher intracellular free Mg^{2+} concentration used in this than previous studies (Brunet et al., 2009). The twice larger A_f than A_s of LTCC (WT) indicates that the O–I_{of} transition predominates over the O–I_{os} transition. Although LTCC (G436R) exhibited significantly larger τ_f and τ_s than LTCC (WT), it showed significantly smaller A_f and larger A_s. Thus, the mutation may more severely impair I_{of} than I_{os} so that I_{os} compensated for the impaired I_{of}. Thus, L_{I-II} may mainly support I_{of}, and the

Please cite this article as: Sheng, X., et al., Two mechanistically distinct effects of dihydropyridine nifedipine on CaV1.2 L-type Ca2+ channels revealed by Timothy syndrome mutation, Eur. J. Pharmacol. (2012), doi:10.1016/j.ejphar.2012.04.029

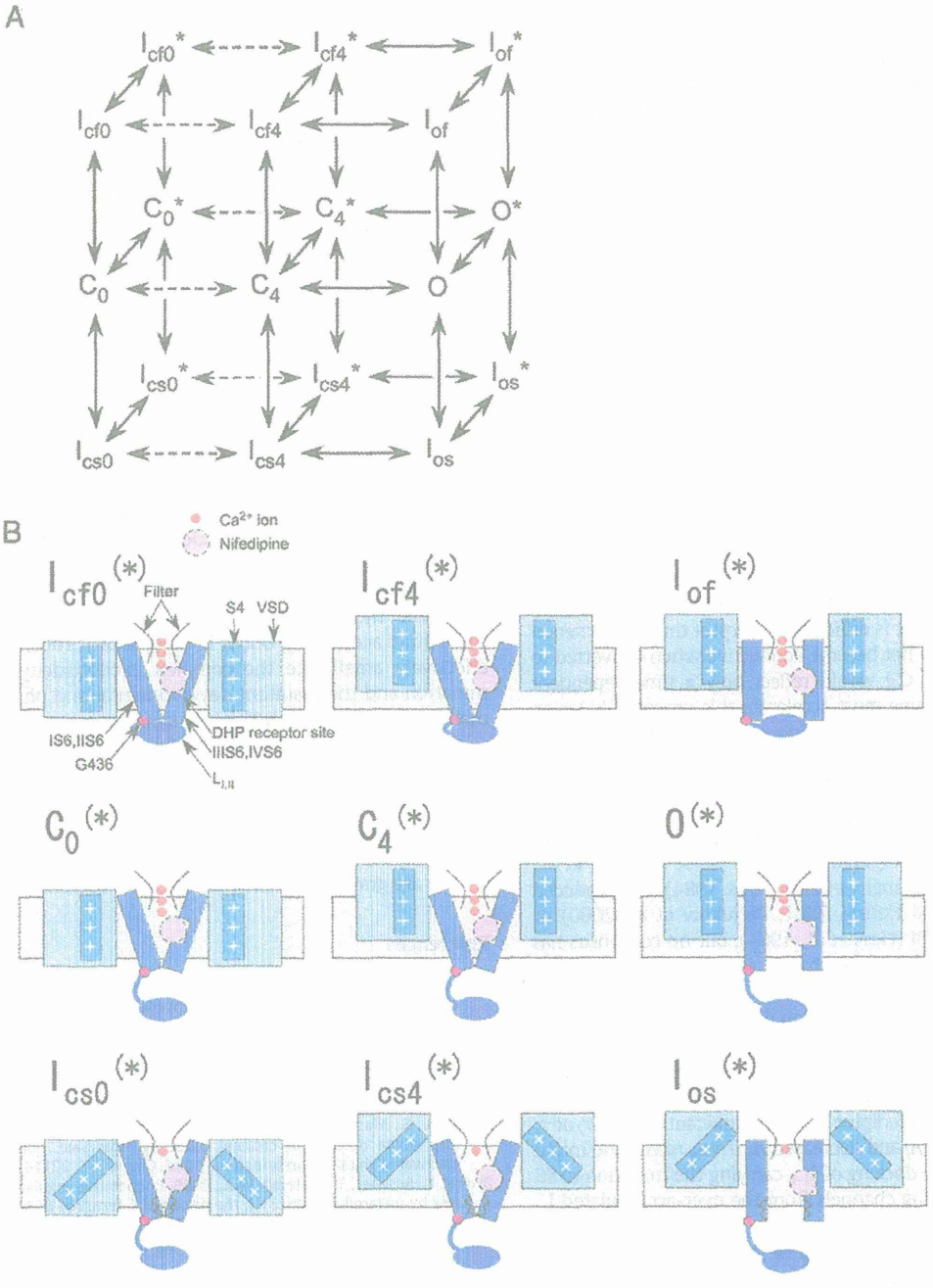

Fig. 7. Allosteric model of L-type Ca^{2+} channels. (A) State diagram of LTCCS. C: closed state; O: open state; I_{cf}: closed fast-inactivated state; I_{cs}: closed slow-inactivated state; I_{of}: open fast-inactivated state; I_{os}: open slow-inactivated state. Asterisks indicate nifedipine-bound states. All interconversions are in principle voltage-dependent. The equilibria and rates for interconversion between nifedipine-free states and between nifedipine-bound states are different. (B) Schematic representation of the side view of LTCCS in the presence and absence of nifedipine. The plasma membrane is depicted as gray squares with the extracellular side upward. Schematics of inner helices formed from I-IVS6, the high-affinity DHP-binding site in III/IVS6, nifedipine, a selectivity filter, Ca^{2+} ions in the selectivity filter, L_{I-II}, G436 and voltage-sensing domains (VSDs) including S4 are shown. The circular DHP-binding site has higher affinity for nifedipine than the square site. Note that the upward movement of VSDs indicates the activation of LTCCs. Fast VDI is shown to be supported by L_{I-II} that occludes the inner mouth of a channel pore by docking to S6. Slow VDI is shown to be associated with gating charge immobilization (indicated by tilted S4), depletion of Ca^{2+} ions in a selectivity filter (indicated by a single Ca^{2+} ion in a filter) and the conformational change of the cytoplasmic part of S6 (indicated by wavy lines). Three Ca^{2+} ions in the selectivity filter indicate conducting states whereas one Ca^{2+} ion in the filter represents non-conducting states.

increased τ_s of LTCC (G436R) may be secondary to the impaired I_{of}. At a voltage step to −100 mV from 0 mV, both channels exhibited biexponential recovery from OSI (Fig. 5), indicating the coexistence of the recovery from I_{of} and I_{os}. Here, we assume that the recovery from I_{of} is faster than that from I_{os} because the recovery was faster after a shorter conditioning pulse in both channels (data not shown). Neither τ_f nor τ_s was significantly different between LTCC (WT) and LTCC (G436R), indicating the similarity in the kinetics of these channels at −100 mV; however, LTCC (G436R) exhibited significantly smaller A_f and larger A_s than LTCC (WT), which probably reflects the difference in A_f and A_s of OSI in the preceding conditional pulse between the channels (Fig. 3).

Fig. 7B schematically illustrates different states of $Ca_V1.2$ subunits. Because the G436R mutation mainly impaired fast CSI and OSI, fast

Please cite this article as: Sheng, X., et al., Two mechanistically distinct effects of dihydropyridine nifedipine on CaV1.2 L-type Ca2+ channels revealed by Timothy syndrome mutation, Eur. J. Pharmacol. (2012), doi:10.1016/j.ejphar.2012.04.029

inactivated states are illustrated to arise from the docking of L_{I-II} to S6 (Fig. 7B) (Stotz and Zamponi, 2001; Stotz et al., 2000). Because slow OSI and CSI were not affected by the mutation, they are shown to be caused by other mechanisms such as the conformational change of VSD, depletion of Ca^{2+} ions in the selectivity filter and/or the conformational change of the cytoplasmic end of S6 (Hadley and Lederer, 1991; Peterson and Catterall, 2006; Shi and Soldatov, 2002; Shirokov et al., 1992). Note that nifedipine bound to $Ca_V1.2$ subunits is also depicted and that different shapes of the DHP receptor represent its state-dependent change in the affinity for nifedipine.

4.3. Comparison of the effects of nifedipine on LTCC (WT) and LTCC (G436R) channels

Nifedipine modified the kinetics of LTCC (WT) and LTCC (G436R) upon depolarization (Figs. 3 and 4) and repolarization (Fig. 5). These effects of nifedipine would reflect a voltage-dependent change in the interaction between LTCC and nifedipine. At −40 mV, nifedipine increased A_f in both channels as reported for other DHPs (Berjukow and Hering, 2001; Berjukow et al., 2000) and abolished the difference in A_f between the channels (Fig. 3), indicating that I_{cf4} has higher affinity for nifedipine than C_4 (Fig. 7B). It is probable that nifedipine allosterically interacts with L_{I-II} which docks to IIIS6 harboring the DHP receptor (Stotz et al., 2000) and thereby augments fast CSI. Nifedipine also decreased τ_s in both channels. It is difficult to interpret this phenomenon if we assume that C_4^* does not become conductive when converted to O^*. If this were the case, CSI would reflect only a time-dependent decrease in C_4, and nifedipine must accelerate this process. However, the nifedipine-induced I_{cs4}–I_{cs4}^* transition cannot accelerate the C_4–I_{cs4}–I_{cs4}^* transition. Thus, we propose that O^* is conductive and that the C_4^*–I_{cs4}^* transition is faster than the C_4–I_{cs4} transition (Fig. 7B).

At 0 mV, nifedipine decreased τ_f in LTCC (WT) (Fig. 4). The acceleration of the decay of LTCC Ba^{2+} currents by DHP antagonists arises from the open-channel block (Handrock et al., 1999; Lacinova et al., 2000; Lee and Tsien, 1983; Sanguinetti and Kass, 1984), drug-induced inactivation (Berjukow and Hering, 2001; Berjukow et al., 2000) or acceleration of intrinsic VDI (Hess et al., 1984), but no consensus has been reached. Because we consider that O^* is conducting, we reject the possibility of the open-channel block and propose that the O^*–I_{of}^* transition is faster than the O–I_{of} transition due to the promoted docking of L_{I-II} to S6. Thus, I_{of} may have higher affinity for nifedipine than O (Fig. 7B). On the other hand, nifedipine did not affect τ_s or A_s in LTCC (WT), suggesting that O and I_{os} have similar affinity for nifedipine (Fig. 7B). In LTCC (G436R), nifedipine did not significantly affect τ_f or τ_s but significantly increased A_f and decreased A_s. Thus, nifedipine might be unable to accelerate the docking of L_{I-II} carrying the mutation to S6 but still capable of recruiting channels from the over-accumulated I_{os} into I_{of}^* in LTCC (G436R).

In the recovery at −100 mV, nifedipine did not affect τ_f in either of the channels (Fig. 5), indicating that I_{cf0} does not have high affinity for nifedipine and thus, is not stabilized by the drug (Fig. 7B). On the other hand, nifedipine significantly increased τ_s in both channels, suggesting that I_{cs0} has higher affinity for nifedipine than C_0 (Fig. 7B). Other DHPs also selectively decelerated the slow component of recovery (Berjukow and Hering, 2001; Berjukow et al., 2000; Lacinova et al., 2000; Sanguinetti and Kass, 1984). Similar τ_f and τ_s of LTCC (WT) and LTCC (G436R) indicate that their kinetics were similar at −100 mV also in the presence of nifedipine. Although nifedipine did not affect A_f or A_s in LTCC (WT), it significantly increased A_f and decreased A_s in LTCC (G436R). This may once again reflect the effect of nifedipine on A_f and A_s of OSI in the conditional pulse (Fig. 3). Thus, a kinetic difference between these channels at a deeply hyperpolarized potential is rather minor, which accounts for the insignificant difference in the tonic block of these channels by nifedipine at −80 mV (Fig. 2).

Taken together, nifedipine promoted fast CSI/OSI at potentials positive to the sub-threshold potential whereas it promoted and stabilized slow CSI at potentials negative to the sub-threshold potential. Hering and his colleagues reported that DHP antagonists (+)- and (−)-isradipine caused an enantioselective tonic block at hyperpolarized potentials but equipotently accelerated the decay of LTCCs at depolarized potentials (Handrock et al., 1999). They found that the former but not the latter effect was disrupted by the mutation of the DHP-binding site in IVS6. Lacinova et al. (2000) showed that the same mutation selectively abolished slow but not fast recovery from VDI in the presence of isradipine. These reports together with the present results suggest that DHP might interact mainly with IIIS5/S6 at depolarized potentials, allosterically modulating the docking of L_{I-II} to IIIS6 and thereby promoting intrinsic fast VDI. On the other hand, DHP might interact mainly with IVS6 at hyperpolarized potentials and allosterically modulate slow VDI.

5. Conclusion

Nifedipine has two mechanistically distinct effects on LTCCs: the promotion of fast CSI/OSI caused by L_{I-II} at potentials positive to the sub-threshold potential and the promotion or stabilization of slow CSI at potentials negative to the sub-threshold potential. These two different mechanisms may underlie the phasic and tonic block of LTCCs by DHP, respectively.

Nifedipine normalized VDI kinetics of LTCCs with the Timothy syndrome mutation. Yarotskyy et al. (2009) also reported that roscovitine accelerates OSI of LTCC (G436R). Thus, these agents may effectively ameliorate the complex excitotoxicity of the Timothy mutation and the resultant developmental and physiological abnormalities in patients with Timothy syndrome.

Supplementary data to this article can be found online at doi:10.1016/j.ejphar.2012.04.029.

Acknowledgement

We are grateful to Ms. Reiko Sakai for secretarial assistance.

References

Barrett, C.F., Tsien, R.W., 2008. The Timothy syndrome mutation differentially affects voltage- and calcium-dependent inactivation of CaV1.2 L-type calcium channels. Proc. Natl. Acad. Sci. U. S. A. 105, 2157–2162.
Bean, B.P., 1984. Nitrendipine block of cardiac calcium channels: high-affinity binding to the inactivated state. Proc. Natl. Acad. Sci. U. S. A. 81, 6388–6392.
Berjukow, S., Hering, S., 2001. Voltage-dependent acceleration of Ca(v)1.2 channel current decay by (+)- and (−)-isradipine. Br. J. Pharmacol. 133, 959–966.
Berjukow, S., Marksteiner, R., Gapp, F., Sinnegger, M.J., Hering, S., 2000. Molecular mechanism of calcium channel block by isradipine. Role of a drug-induced inactivated channel conformation. J. Biol. Chem. 275, 22114–22120.
Brunet, S., Scheuer, T., Catterall, W.A., 2009. Cooperative regulation of Ca(v)1.2 channels by intracellular Mg(2+), the proximal C-terminal EF-hand, and the distal C-terminal domain. J. Gen. Physiol. 134, 81–94.
Catterall, W.A., 2000. Structure and regulation of voltage-gated Ca2+ channels. Annu. Rev. Cell Dev. Biol. 16, 521–555.
Hadley, R.W., Lederer, W.J., 1991. Properties of L-type calcium channel gating current in isolated guinea pig ventricular myocytes. J. Gen. Physiol. 98, 265–285.
Handrock, R., Rao-Schymanski, R., Klugbauer, N., Hofmann, F., Herzig, S., 1999. Dihydropyridine enantiomers block recombinant L-type Ca2+ channels by two different mechanisms. J. Physiol. 521 (Pt 1), 31–42.
Hering, S., Berjukow, S., Sokolov, S., Marksteiner, R., Weiss, R.G., Kraus, R., Timin, E.N., 2000. Molecular determinants of inactivation in voltage-gated Ca2+ channels. J. Physiol. 528 (Pt 2), 237–249.
Herlitze, S., Hockerman, G.H., Scheuer, T., Catterall, W.A., 1997. Molecular determinants of inactivation and G protein modulation in the intracellular loop connecting domains I and II of the calcium channel alpha1A subunit. Proc. Natl. Acad. Sci. U. S. A. 94, 1512–1516.
Hess, P., Lansman, J.B., Tsien, R.W., 1984. Different modes of Ca channel gating behaviour favoured by dihydropyridine Ca agonists and antagonists. Nature 311, 538–544.
Hockerman, G.H., Peterson, B.Z., Johnson, B.D., Catterall, W.A., 1997. Molecular determinants of drug binding and action on L-type calcium channels. Annu. Rev. Pharmacol. Toxicol. 37, 361–396.
Kammann, M., Laufs, J., Schell, J., Gronenborn, B., 1989. Rapid insertional mutagenesis of DNA by polymerase chain reaction (PCR). Nucleic Acids Res. 17, 5404.
Kobrinsky, E., Kepplinger, K.J., Yu, A., Harry, J.B., Kahr, H., Romanin, C., Abernethy, D.R., Soldatov, N.M., 2004. Voltage-gated rearrangements associated with differential

Please cite this article as: Sheng, X., et al., Two mechanistically distinct effects of dihydropyridine nifedipine on CaV1.2 L-type Ca2+ channels revealed by Timothy syndrome mutation, Eur. J. Pharmacol. (2012), doi:10.1016/j.ejphar.2012.04.029

beta-subunit modulation of the L-type Ca(2+) channel inactivation. Biophys. J. 87, 844–857.
Lacinova, L., Klugbauer, N., Hofmann, F., 2000. State- and isoform-dependent interaction of isradipine with the alpha1C L-type calcium channel. Pflugers Arch. 440, 50–60.
Lee, K.S., Tsien, R.W., 1983. Mechanism of calcium channel blockade by verapamil, D600, diltiazem and nitrendipine in single dialysed heart cells. Nature 302, 790–794.
Peterson, B.Z., Catterall, W.A., 2006. Allosteric interactions required for high-affinity binding of dihydropyridine antagonists to Ca(V)1.1 Channels are modulated by calcium in the pore. Mol. Pharmacol. 70, 667–675.
Raybaud, A., Dodier, Y., Bissonnette, P., Simoes, M., Bichet, D.G., Sauve, R., Parent, L., 2006. The role of the GX9GX3G motif in the gating of high voltage-activated Ca2 + channels. J. Biol. Chem. 281, 39424–39436.
Sanguinetti, M.C., Kass, R.S., 1984. Voltage-dependent block of calcium channel current in the calf cardiac Purkinje fiber by dihydropyridine calcium channel antagonists. Circ. Res. 55, 336–348.
Shi, C., Soldatov, N.M., 2002. Molecular determinants of voltage-dependent slow inactivation of the Ca2+ channel. J. Biol. Chem. 277, 6813–6821.
Shirokov, R., Levis, R., Shirokova, N., Rios, E., 1992. Two classes of gating current from L-type Ca channels in guinea pig ventricular myocytes. J. Gen. Physiol. 99, 863–895.
Soldatov, N.M., 2003. Ca2+ channel moving tail: link between Ca2+-induced inactivation and Ca2+ signal transduction. Trends Pharmacol. Sci. 24, 167–171.
Splawski, I., Timothy, K.W., Sharpe, L.M., Decher, N., Kumar, P., Bloise, R., Napolitano, C., Schwartz, P.J., Joseph, R.M., Condouris, K., Tager-Flusberg, H., Priori, S.G., Sanguinetti, M.C., Keating, M.T., 2004. Ca(V)1.2 calcium channel dysfunction causes a multisystem disorder including arrhythmia and autism. Cell 119, 19–31.
Splawski, I., Timothy, K.W., Decher, N., Kumar, P., Sachse, F.B., Beggs, A.H., Sanguinetti, M.C., Keating, M.T., 2005. Severe arrhythmia disorder caused by cardiac L-type calcium channel mutations. Proc. Natl. Acad. Sci. U. S. A. 102, 8089–8096 (discussion 8086–8088).
Stotz, S.C., Zamponi, G.W., 2001. Structural determinants of fast inactivation of high voltage-activated Ca(2+) channels. Trends Neurosci. 24, 176–181.
Stotz, S.C., Hamid, J., Spaetgens, R.L., Jarvis, S.E., Zamponi, G.W., 2000. Fast inactivation of voltage-dependent calcium channels. A hinged-lid mechanism? J. Biol. Chem. 275, 24575–24582.
Stotz, S.C., Jarvis, S.E., Zamponi, G.W., 2004. Functional roles of cytoplasmic loops and pore lining transmembrane helices in the voltage-dependent inactivation of HVA calcium channels. J. Physiol. 554, 263–273.
Yamada, M., Ohta, K., Niwa, A., Tsujino, N., Nakada, T., Hirose, M., 2008. Contribution of L-type Ca2+ channels to early afterdepolarizations induced by I Kr and I Ks channel suppression in guinea pig ventricular myocytes. J. Membr. Biol. 222, 151–166.
Yarotskyy, V., Gao, G., Peterson, B.Z., Elmslie, K.S., 2009. The Timothy syndrome mutation of cardiac CaV1.2 (L-type) channels: multiple altered gating mechanisms and pharmacological restoration of inactivation. J. Physiol. 587, 551–565.
Zuhlke, R.D., Pitt, G.S., Deisseroth, K., Tsien, R.W., Reuter, H., 1999. Calmodulin supports both inactivation and facilitation of L-type calcium channels. Nature 399, 159–162.

Please cite this article as: Sheng, X., et al., Two mechanistically distinct effects of dihydropyridine nifedipine on CaV1.2 L-type Ca2+ channels revealed by Timothy syndrome mutation, Eur. J. Pharmacol. (2012), doi:10.1016/j.ejphar.2012.04.029

Childs Nerv Syst
DOI 10.1007/s00381-012-1891-9

TECHNICAL NOTE

Use of magnetic resonance imaging to identify the edge of a dural tear in an infant with growing skull fracture: a case study

Hideki Matsuura · Shinichi Omama · Yuki Yoshida · Shunrou Fujiwara · Takayuki Honda · Manami Akasaka · Atsushi Kamei · Kuniaki Ogasawara

Received: 5 July 2012 / Accepted: 3 August 2012

Abstract
Purpose Growing skull fractures can be a challenging surgical problem facing pediatric neurosurgeons. The goal of this manuscript was to describe an effective surgical method used to treat a growing skull fracture.
Methods We present a case study of a 2-month-old boy who fell from his mother's arms and hit his head on the floor; he underwent X-ray, magnetic resonance (MR), and computed tomography (CT) imaging before cranioplasty with dural plasty.
Results X-ray performed on admission revealed a diastatic fracture with a gap of 8 mm in the right frontal bone and a linear fracture in the right occipital bone. X-ray performed 37 days after injury demonstrated that the gap had increased to 25 mm, and the patient was diagnosed with a growing skull fracture of the right parietal bone. Cranioplasty with dural plasty was performed on day 39. A combination of MR and CT images enabled the edge of the dural tear to be plotted on a three-dimensional image of the skull, and this was used to estimate the location of the edge of the dural tear on the scalp.
Conclusions We achieved excellent outcomes in terms of bony coverage and dural plasty. The combination of MR and CT images may be recommended for surgical repair of growing skull fracture in children.

Keywords Growing skull fracture · Enhanced MR imaging · Dural plasty · Cranioplasty

H. Matsuura (✉) · S. Fujiwara · K. Ogasawara
Department of Neurosurgery, Iwate Medical University,
Uchimaru 19-1,
Morioka 020-8505, Japan
e-mail: hidekima@iwate-med.ac.jp

S. Omama · Y. Yoshida
Department of Critical Care and Emergency Center,
Iwate Medical University,
Uchimaru 19-1,
Morioka 020-8505, Japan

T. Honda
Department of Plastic and Reconstructive Surgery,
Iwate Medical University,
Uchimaru 19-1,
Morioka 020-8505, Japan

M. Akasaka · A. Kamei
Department of Pediatrics, Iwate Medical University,
Uchimaru 19-1,
Morioka 020-8505, Japan

Introduction

Growing skull fractures are an uncommon complication of pediatric head trauma. The reported incidence of growing skull fractures ranges from 0.05 to 1.6 % [1]. The standard surgical treatment of the lesion involves repair of the dural defect with a graft and cranioplasty [3, 4]. The dural defect is usually larger than the bony defect; therefore, craniotomy around the fracture site is necessary, resulting in wider craniotomy [5]. Identifying the edge of the dural tear in presurgical planning may allow the area of the craniotomy to be minimized. The dura is enhanced by gadolinium on T1-weighted magnetic resonance (MR) images. Here, we describe a case of an infant with a growing skull fracture in which MR

Published online: 16 August 2012

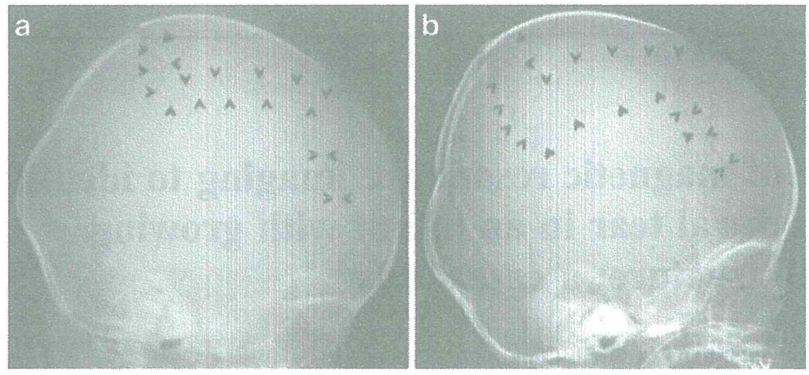

Fig. 1 **a** Lateral skull radiograph taken on initial presentation to hospital (day of accident). A diastatic right parietal skull fracture is evident, indicated by the *black arrowheads*. **b** Lateral skull radiograph taken 37 days after the accident. Enlargement of the fracture is evident, indicated by the *black arrowheads*

imaging with gadolinium enhancement was used to identify the edge of the dural tear. We use this case report to describe an effective surgical method for growing skull fractures.

Case report

A 2-month-old boy fell from his mother's arms and hit his head on the floor. Six hours later, he was transferred to our hospital. On admission, he presented with a small swelling in the right parietotemporal region. No consciousness disturbance or neurological deficits were observed. Plain cranial X-ray revealed a diastatic fracture with a gap of 8 mm in the right frontal bone and a linear fracture in the right occipital bone (Fig. 1a). Head computed tomography (CT) showed a thin subdural hematoma in the bilateral cerebral hemispheres. The patient's course was uneventful until the tenth day of hospitalization, when a bulge appeared in the right frontoparietal region. This bulge became progressively larger and firmer. Plain cranial X-ray performed 37 days after the onset of the head injury demonstrated that the bone defect had widened and the gap had increased to 25 mm (Fig. 1b). A CT scan revealed a leptomeningeal cyst herniating through the bone defect. Based on these findings, the patient was diagnosed with a growing skull fracture.

Prior to craniotomy to repair the lesion, the patient underwent MR imaging with gadolinium enhancement and three-dimensional CT. T1-weighted MR images showed the edge of the skull fracture as a discontinuity of the high-intensity signal from the bone marrow and the edge of the dural tear as discontinuity of gadolinium enhancement (Fig. 2). The distance between the edge of the skull fracture and the edge of the dural tear was measured on each slice, the thickness of which was 6.4 mm. The edge of the skull fracture identified on each MR image slice was identified on each corresponding CT image slice, and the edge of the dural tear was plotted on the reconstructed three-dimensional skull CT images based on the measurement from the MR images (Fig. 3).

After induction of general anesthesia, the edge of the growing skull fracture was identified on the scalp using manual palpitation, and the estimated edge of the dural tear was marked on the scalp using the reconstructed three-dimensional skull CT images (Fig. 4a). A skin incision was made, and the pericranial tissue corresponding to the area of the estimated edge of the dural tear was stripped. Craniotomy was performed with a margin of 1 cm for the estimated edge of the dural tear. The organized connective tissue was observed in the skull defect, and the spatial relation between craniotomy and the edge of the dural tear corresponded with the preoperatively estimated relation

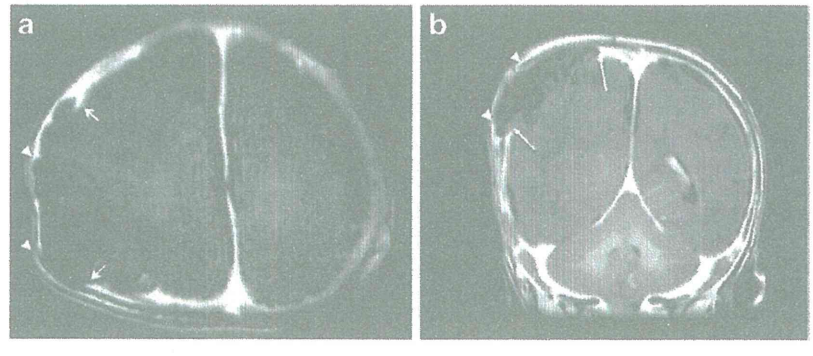

Fig. 2 **a** Axial enhanced T1-weighted MR image shows enhancement of dural tear (*arrow*) and the edge of skull fracture as discontinuity of high signal of the bone marrow (*arrow head*). **b** Coronal enhanced T1-weighted MR image shows enhancement of dural tear (*arrow*) and the edge of skull fracture as discontinuity of high signal of the bone marrow (*arrowhead*)

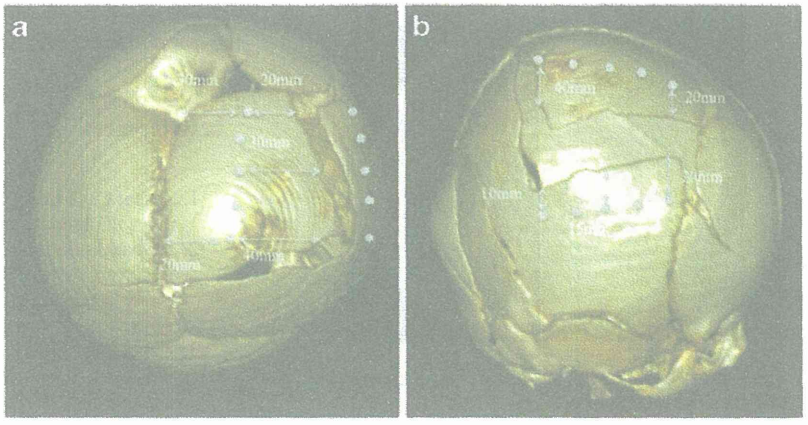

Fig. 3 Three-dimensional computed tomography images (**a**, **b**) showing distance measurements to the dural defect at the end of the bone

(Fig. 4b). The dural defect was covered with the stripped pericranial tissue (Fig. 4c), and cranioplasty was performed using the skull segmented on several pieces. The postoperative course was uneventful. A CT scan 1 year after surgery demonstrated a resolution of the growing skull fracture (Fig. 5).

Discussion

In the present case of a growing skull fracture, the edge of the skull fracture and the edge of the dural tear were identified from T1-weighted MR images [7]. This enabled the spatial relation between the two components to be identified. A combination of MR and CT images enabled the edge of the dural tear to be plotted on a three-dimensional image of the skull, and this was used to estimate the location of the edge of the dural tear on the scalp. As a result, the intraoperative spatial relation between craniotomy and the edge of the dural tear corresponded with the preoperatively estimated relation, and the area of the skin incision and craniotomy was minimized.

The autologous pericranial graft used in the repair of dural defects is histocompatible, less allergenic, well

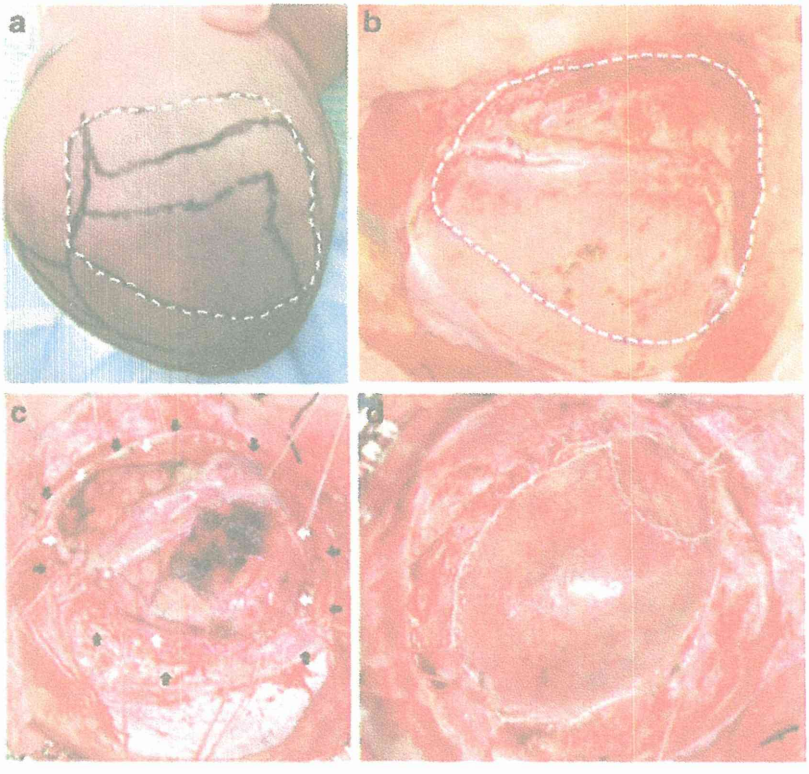

Fig. 4 **a** Photograph of the head of the patient prior to surgery. The *white dashed line* indicates the position of the dural defect over the temporal and parietal areas. **b** Photograph taken after the pericranial tissue had been dissected and the galeal tissue, adherent to the underlying bone defect. The *white dashed line* corresponds to the same area as in **c**. **c** Photograph taken after the galeal tissue adherent to the underlying bone defect and bone had been cut. *White arrows* indicate the outline of the dural defect. *Black arrows* indicate the bone flap margin. **d** Photograph showing the closure of the dural defect by pericranial graft

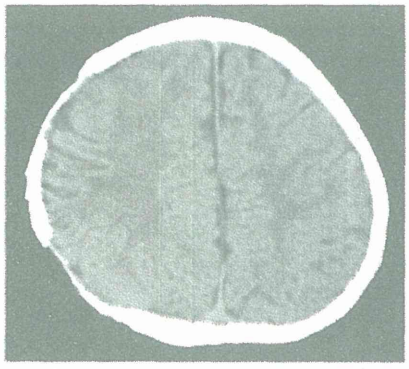

Fig. 5 Axial plain CT showing the expansion of the cerebral hemisphere and smooth bonding of the edge

vascularized and heals within the surrounding tissue [2]. In the present case, the pericranial graft was stripped in an area corresponding to the estimated edge of the dural tear, facilitating a minimal area of stripped pericranium.

In general, neuronavigation is used in an attempt to address growing skull fractures. However, children are less able than adults to tolerate the rigid head fixation required for the neuronavigation systems [6]. In particular, the use of a head clamp is inappropriate in children under 2 years of age [6]. The combination of MR and CT images may be recommended for surgical repair of growing skull fracture in children.

References

1. Arseni C, Civrea AV (1981) Clinicotherapeutic aspects in the growing skull fracture: a review of the literature. Childs Brain 8:161–172
2. Bashar A, Saffet T, Bulent C, Odhan Y, Banu T, Galip ZS (2009) Reconstruction of growing skull fracture with in situ galeal duraplasty and porous polyethylene sheet. J Craniofac Surg 20:1245–1249
3. Gupta SK, Reddy NM, Khosla VK, Mathuriya SN, Shama BS, Pathak A, Tewari MK, Kak VK (1997) Growing skull fractures: a clinical study of 41 patients. Acta Neurochir (Wine) 139:928–932
4. Halliday AC, Chapman PH, Heros RC (1990) Leptomeningeal cyst resulting from adulthood trauma: case report. Neurosurgery 26:150–153
5. Ziyal IM, Aydin Y, Turkmen CS, Salas E, Kaya AR, Ozveren F (1998) The natural history of late diagnosis or untreated growing skull fractures: report on two cases. Acta Neurochir (Wine) 140:651–654
6. Simon C, Mehapral S, Caroline H, Jothi K, Michael J, Maggie L, Conor M (2008) The use of noninvasive electromagnetic neuronavigation for slit ventricle syndrome and complex hydrocephalus in a pediatric population. J Neurosurg Pediatris 2:430–434
7. Vogler JB III, Murphy WA (1988) Bone marrow imaging. Radiology 168:679–693